Preheat-enhanced laminar burning velocity and nitrogen-chemistry interactions of ammonia/n-heptane/air flames

Zhichao Zhou[a,b], Danan Chen[a*], Junqing Zhang[a,b], Shusen Lin[a,b], Xing Li[a,b], Agustin Valera-Medina[c], Jun Li[a,b,d*]

[a] *Guangzhou Institute of Energy Conversion, Chinese Academy of Sciences, Guangzhou 510640, China*

[b] *School of Energy Science and Engineering, University of Science and Technology of China, Guangzhou 510640, China*

[c] *College of Physical Sciences and Engineering, Cardiff University, Cardiff, CF24 3AA, United Kingdom*

[d] *Jiangxi Carbon Neutralization Research Center, Jiangxi Academy of Sciences, Nanchang, Jiangxi, 330096, China*

Corresponding author

*Danan Chen, E-mail: chendn@ms.giec.ac.cn

*Jun Li, E-mail: lijun@ms.giec.ac.cn

Abstract

Co-combustion of ammonia with hydrocarbons introduces complex carbon-nitrogen (C-N) chemical interactions that critically govern flame propagation and pollutant formation, yet the underlying kinetic mechanisms remain poorly elucidated due to a scarcity of reliable experimental data under elevated temperature. This study aims to resolve these C-N interactions by integrating laminar burning velocity (LBV) measurements with a purpose-built skeletal kinetic model that explicitly captures the cross-reactivity between carbonaceous and nitrogenous species. LBV of n-heptane/ammonia/air mixtures were experimentally determined using the externally heated divergent channel (EHDC) method over a wide parameter space: preheat temperatures of 400–500 K, equivalence ratios of 0.8–1.2, and ammonia fractions up to 70%. The updated skeletal mechanism incorporating a refined NH_2 sub-mechanism and C-N coupling chemistry performs well under high ammonia blending ratios and elevated temperature conditions, achieving a 5% improvement in predictive accuracy for LBV. With increasing ammonia fraction, the LBV undergoes a two-stage reduction, declining near-linearly below 50% ammonia and transitioning to exponential decay at higher fractions. This shift is mechanistically linked to the changing kinetic dominance from carbon-driven to nitrogen-driven pathways. The LBV peaks under slightly rich conditions (Φ = 1.1), owing to the synergistic effects of adiabatic flame temperature and enhanced radical pooling involving carbon and nitrogen species. Raising the preheat temperature from 400 K to 500 K enhances the LBV by approximately 50%. Reaction pathway analysis further identifies HCN as the pivotal

intermediate bridging the carbon and nitrogen chemistry, with its formation route switching from carbon-involving to nitrogen-dominated pathways as the equivalence ratio increases. By establishing a direct connection between macroscopic combustion parameters and the underlying kinetic interactions, this work provides both an experimental benchmark and a validated kinetic framework for advancing ammonia–hydrocarbon dual-fuel combustion mod.

Keywords: Ammonia flame; n-Heptane; Laminar burning velocity; Chemical kinetic analysis; C-N reaction pathway

1. Introduction

Against the backdrop of diminishing proven fossil fuel reserves and escalating global energy demand, controlling carbon emissions allowances from conventional hydrocarbon fuels has emerged as a critical challenge in the current global energy transition. The development of zero-carbon ammonia-hydrogen energy demonstrates significant advantages in reducing carbon emissions and enhancing energy utilization efficiency [1]. Compared to hydrogen fuel, ammonia offers distinct advantages in terms of cost-effectiveness, transportation, storage, and safety. Owing to its superior volumetric energy density and high octane number, it has been identified as a promising alternative fuel for internal combustion engines [2]. However, in practical applications, ammonia exhibits slow flame speed, prolonged ignition delay, and flame instability [3]. The laminar burning velocity (LBV) of pure ammonia at atmospheric pressure and temperature is merely around 7 cm/s. This characteristic renders it challenging to utilize as a standalone fuel [4]. A more viable combustion strategy involves the use of highly reactive fuels, such as diesel, for pilot ignition. Consequently, the ammonia-diesel dual-fuel mode holds considerable promise as a forward-looking solution for high-power and long-duration energy storage applications, notably in deep-sea vessels [5] and heavy machinery [6].

To enable high-fidelity combustion simulations of ammonia-diesel dual-fuel modes, the development of CFD-applicable mechanisms remains a focal point of research [7]. While diesel fuel is a complex hydrocarbon mixture comprising alkanes, aromatics, cycloalkanes, and other species—each exhibiting distinct chemical and physical properties. Owing to its relatively high cetane number, favorable hydrogen-to-carbon (H/C) ratio, and excellent ignition characteristics, n-heptane is widely adopted as a diesel surrogate and a key component of multi-component reference fuels [8, 9]. To date, investigations into the kinetics of ammonia/n-heptane reactions have established a pivotal theoretical foundation for modeling the combustion dynamics inherent to dual-fuel internal combustion engines application [10]. Table 1 summarizes recent studies on ammonia/n-heptane reaction mechanisms. Yu et al. [11] initially measured ignition delay times (IDT; 635–945 K, 10–15 bar) of n-heptane/ammonia blends in a rapid compression machine (RCM) and proposed a hybrid mechanism integrating the n-heptane sub-mechanism from Zhang et al. [12] with ammonia

chemistry from Glarborg et al. [13]. Subsequent studies have progressively refined this framework: Pan et al. [14] updated elementary reaction rates using jet-stirred reactor (JSR) data; Thorsen et al. [15] expanded validation to broader conditions (400–900 K, 21–100 bar); Dong et al. [16] further optimized the ammonia sub-mechanism against high-pressure shock tube (HPST) measurements (1000–1400 K, 10 bar), while Fang et al. [17] validated under higher-temperature conditions (1350–1500 K, 2 atm). To reduce computational cost, Xu et al. [18] derived a skeletal mechanism comprising 69 species and 389 reactions. Alekseev and Nilsson. [19] and Ou et al. [20] independently developed compact mechanisms suitable for CFD applications. More recently, Mao et al. [21] introduced a data-driven surrogate model for ignition delay prediction, significantly reducing the computational demands of detailed kinetics. Despite these advancements, current mechanistic studies predominantly rely on established n-heptane skeletal frameworks, with validation efforts primarily focused on IDT. Comprehensive experimental characterization, particularly LBV measurements across wide parametric ranges, remains comparatively limited, constraining robust validation of kinetic models across diverse combustion regimes.

High-precision LBV experimental data is of vital importance for the reliable verification of dynamic models and the development of prediction models with low uncertainty [22, 23]. Commonly employed techniques for laminar burning velocity measurements include the Bunsen burner method [24], counterflow flame method [25], heat flux method [26, 27], spherical flame method [28], and diverging channel method [29]. While extensive LBV investigations have been conducted on n-heptane, substantial physicochemical disparities between blended fuel components have led to limited experimental LBV data availability for ammonia-blended n-heptane premixtures. Lubrano Lavadera et al. [30] pioneered LBV measurements of ammonia/n-heptane blends at atmospheric pressure and 338 K using the heat flux method. For an ammonia concentration of over 80% and a pressure of 1 MPa, Liu et al. [31] obtained experimental data using the spherical flame method at 373 K. Subsequently, Guo et al. [28] measured the laminar burning velocities of these blends at 393 K and 0.3 MPa with ammonia blending fractions of 0.4, 0.6, and 0.8 through the same method, thereby validating the chemical kinetic mechanism proposed by Xu et al. [18]. Conventional constant-volume combustion chambers face difficulties in achieving high-temperature premixing and maintaining stable laminar flames, making LBV experimental data at elevated temperatures (>400 K) remain scarce. Experimental data across wide ranges of ammonia blending ratios and equivalence ratios are, however, of paramount importance for further elucidating variations in the C-N interaction pathways of blended fuels.

Table 1 Summary of Mechanism Study on Ammonia/n-Heptane

Authors	Species	Reaction	Validation	Year	Refs
Yu L et al.	1376	6499	RCM	2020	[11, 32]
Lubrano Lavadera et al.	299	8028	heat flux method	2020	[30]

Dong S et al.	2854	11790	HPST	2022	[16]
Pan J et al.	1375	6535	JSR	2023	[14]
Thorsen S et al.	1376	6499	ST	2023	[15]
Xu L et al.	69	389	ST,RCM,JSR	2023	[18]
Wang B et al.	74	495	ST,RCM	2023	[33]
Fang Y et al.	2860	11892	HPST	2024	[17]
Alekseev A et al.	57	159	JSR	2024	[19]
Liu B et al.	205	1195	LBV	2024	[31]
Ji Z et al.	1300	5630	ST,RCM	2025	[34]
Wang H et al.	84	422	IDT,LBV,JSR	2025	[35]
Ou J et al.	68	377	RCM,HPST	2025	[20]

C-N interaction reactions influence the formation and consumption of CO and NO, thereby affecting flame structure and pollutant emissions [36]. In the LBV pathway analysis of $C_3H_8/H_2/N_2O/Ar$ mixtures under ambient conditions, Ge et al. [37] demonstrated that C-N interaction reactions HCO + NO = CO + HNO and CO + NO_2 = CO_2 + NO play vital roles within the reaction pathways. Research on ammonia/ethylene co-flow diffusion flames indicates that a 5% ammonia doping will cause a strong coupling between carbon and nitrogen species, promoting NO conversion and suppressing soot formation through C-N intermediate products such as HCN and CH_2NH [38], while the potential damaging effect of C-N interactions on the key formation pathways of soot remains unclear [39]. While current research has identified the primary intermediates of the C-N reaction and elucidated its impact on flame properties, a systematic explanation for the changing trends in C-N reaction pathways under varying ammonia fractions and equivalence ratios remains absent.

This study employs the externally heated diverging channel (EHDC) method to determine LBV of n-heptane/ammonia fuels across extensive parameter ranges. Experimental conditions cover preheat temperatures (T_u) of 400–500 K, equivalence ratios (Φ) of 0.8–1.2, and ammonia blending fractions (X_{NH3}) from 0 to 70%, thereby addressing critical gaps in existing experimental LBV datasets. Leveraging experimentally validated modeling, this work scrutinizes C-N interactions and NH_2 sub-mechanism in blended fuels, offering novel insights into the intrinsic mechanisms governing LBV variations in fuel mixtures. Furthermore, it provides targeted support for developing reaction mechanisms in ammonia-diesel applications, particularly regarding reaction networks and reactivity regulation of preheated fuel mixture .

2. Methodology

2.1 Reaction kinetic mechanism

Elucidating the underlying chemistry through kinetic modeling is central to understanding the combustion behavior of ammonia/n-heptane blends. This study adopts a skeletal mechanism modified from Wang [33], which has been extensively employed for performance prediction of engines operating under ammonia-diesel dual-fuel modes [40-42]. Wang et al. [33] integrated the well-validated skeletal n-heptane mechanisms by Chang et al. [43] and NUIGMech1.2 [12], coupled with refined ammonia chemistry from Stagni et al. [44] and their previously established interaction chemistry, to develop a detailed mechanism comprising 184 species and 1,094 reactions. Critical reactions governing low-temperature n-heptane oxidation within the skeletal mechanism, such as $NC_7H_{16} + OH <=> C_7H_{15} + H_2O$, were optimized to enhance first-stage ignition prediction accuracy. Subsequent reduction via directed relation graph with error propagation (DRGEP) and sensitivity analysis yielded a skeletal ammonia/n-heptane mechanism with 74 species and 495 reactions. It is note that foundational work investigated C-N interaction pathways, identifying the reaction $n\text{-}C_7H_{16} + NH_2 <=> C_7H_{15}\text{-}1/C_7H_{15}\text{-}2/C_7H_{15}\text{-}3/C_7H_{15}\text{-}4 + NH_3$ as critically influential in low-to-intermediate temperature oxidation of ammonia/n-heptane mixtures. Thorsen et al. [15] later modified the rate coefficients for these reactions. Current research confirmed that a subset of C-N reactions is essential for accurate ignition and combustion prediction in dual fuels, yet comprehensive characterization of these pathways has only recently emerged. Early mechanisms neglecting such interaction chemistry exhibited significant predictive deviations [18]. While the Wang mechanism incorporates key advances, it omits recent refinements to C-N interactions and NH_2 reaction pathways. To address this, the C-N kinetic model in this study incorporates relevant reactions proposed by Alekseev et al. [19] from Lund University to enhance the accuracy of LBV predictions under high-temperature conditions. The selection and modification of rate constants were based on recent studies. Specifically, the update for R403 is supported by discussions from Zhan et al. [45] and Zhang et al [46], who highlighted the significant role of HCO in C-N interactions and LBV. In addition to parameter updates, R400 $CH_2O + NH_2 = HCO + NH_3$ and R403 $HCO + HNO = H_2NO + CO$ were added to the present mechanism. They are H-transfer reactions that contribute key formaldehyde/formyl interactions with nitrogen radicals, significantly influencing intermediate species concentrations.These modifications to the C-N reaction mechanism are also considered to play a significant role in the CFD simulation of dual-fuel engines [20]. Consequently, this study implements parameter revisions for relevant reactions, with specific adjustments systematically documented in Table 2. The updated mechanism is presented in the supplementary materials.

Table 2 Mechanism optimization parameters
(*represents a deviation from the original mechanism)

Reactions	A	n	Ea	Source
C-N interaction reactions				
R395 $CO + N_2O = CO_2 + N_2$	2.510E14	0	46000.0	[19]
R400* $CH_2O + NH_2 = HCO + NH_3$	6.3E04	3.0	3770.0	[47]

Reactions	A	n	Ea	Source
R403* HCO + HNO = H_2NO + CO	4.9E01	3.27	1754	[47]
R411 CH_4+ NH_2 = CH_3 + NH_3	1500.0	3.01	9940.0	[19]
R488 C_2H_4 + NH_2 = C_2H_3 + NH_3	1.17E13	0	10274	[19]
R492 n-C_3H_7CHO + NH_2 = n-C_3H_7CO + NH_3	4.74E04	3.0	4670.0	[19]
R495 n-C_7H_{16} + NH_2 = C_7H_{15} + NH_3	34.68	3.5833	2948.82	[19]
NH_2 sub reactions				
R236* NH_2 + HO_2= HNO + H_2O	2.2E09	0.7906	-1428	[48]
R237 NH_2 + HO_2 = NH_3 + O_2	5.9E07	1.592	-1373	[48]
R238 NH_2 + HO_2 = H_2NO + OH	1.0E12	0.1662	-938	[48]
R244 NH_2 + NO_2= N_2O + H_2O	4.3E17	-1.874	588	[45]

The reaction pathways involving NH_2 are pivotal in determining the reactivity of NH_3, with Stagni et al. [44] previously identifying NH_3 + O_2 = NH_2 + HO_2 as the dominant channel. More recently, Klippenstein et al. [48], employing high-accuracy quantum chemical calculations, identified the reverse reaction NH_2 + HO_2 = NH_3 + O_2 as the primary pathway. Zhang et al. [46] compared the rate coefficients from these studies and demonstrated that the most significant discrepancies arise below 500 K. Hence, R236 was added as an important chain termination reaction for generating H_2O and NH_2 oxidation. The kinetic parameters proposed by Klippenstein et al. [48] exhibit lower uncertainty and are grounded in a more comprehensive theoretical framework, which derived from high-level quantum chemistry calculations, necessitating an update to the corresponding reaction rates in the present mechanism. The revised mechanism comprises 74 species and 498 reactions, with its structural architecture illustrated in Fig. 1.

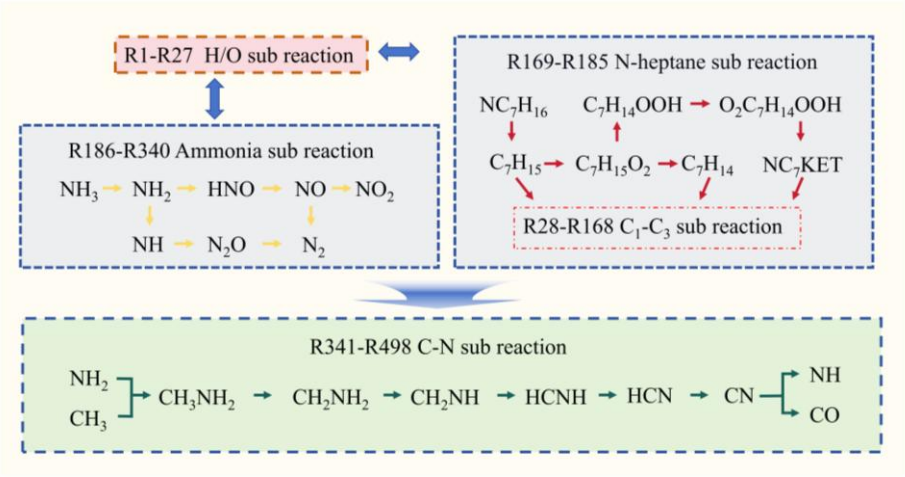

Fig. 1 Mechanism structure diagram

In present numerical research, CHEMKIN-PRO was employed to simulate a steady, one-dimensional, freely propagating laminar premixed flame.The aim was to explore the possible coupling effects under different equivalence ratios, initial temperatures, and ammonia volume

compositions.The computational region was defined with a length of 10 cm after validation. The upper limit for the number of grid points was set at 1000, while the lower limit for the number of adaptive grid intervals was fixed at 10. To guarantee mesh independence, adaptive re-meshing was applied to each simulation scenario. The gradient (GRAD) and curvature (CURV) criteria for this re-meshing process were specified as 0.1 and 0.02, respectively. Grid independence studies confirm that the current grid configuration demonstrates high robustness, with no significant changes in computational outcomes observed upon further grid refinement. Moreover, all simulations took into consideration both the Soret effect and the mixture-averaged transport properties to achieve higher computational efficiency while maintaining accuracy. The zero-dimensional (0 D) homogeneous reactor model was employed to compute the ignition delay times (IDT). In the IDT simulations for RCM experiments, the temporal evolution of volume was not incorporated and constant-volume was adopted, as this aspect falls outside the scope of the present investigation.

2.2 Experimental setup

For this study, the EHDC method was employed to measure the LBV. The schematic diagram of the experimental setup is presented in Fig. 2. This method has been extensively verified for determining hydrocarbon fuel LBV [49-52].

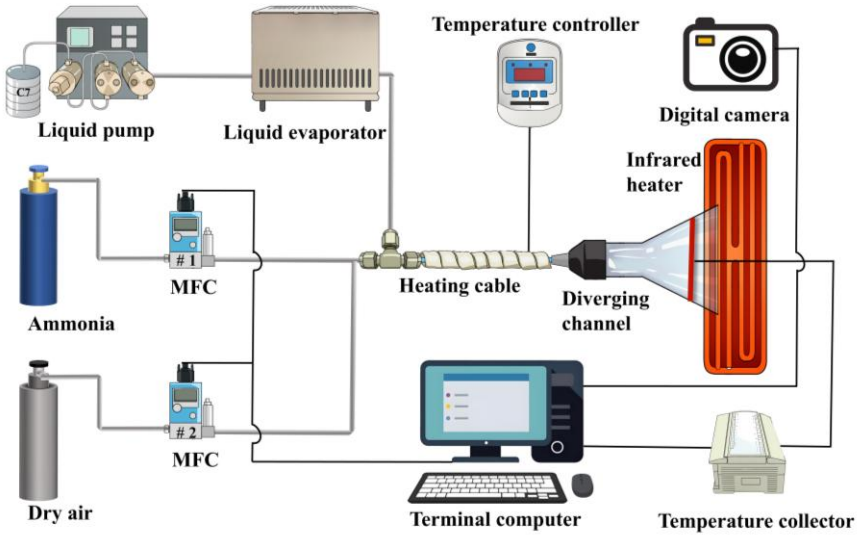

Fig. 2 Schematic experimental setup

For a detailed introduction of this apparatus, please refer to our previous work [53]. Here, only a brief introduction to the experimental principle is provided. An expanding quartz channel with an aspect ratio of 12.5 and a divergence angle of 15° was utilized.This specific geometric shape of the channel ensures a uniform distribution of velocity and temperature perpendicular to the flow direction. Dry air and ammonia were supplied from steel cylinders, and their flow rates were precisely controlled using commercial mass flow meters with an accuracy of ±1% of the full scale range. The liquid fuel, n-heptane, was delivered by a high pressure piston pump. This pump can continuously dispense the liquid at a constant volumetric flow rate ranging from 0.01 to 10 ml/min.

Based on the measurement accuracy of pump and mass flow controller, the measurement error of the equivalent ratio was calculated to below ±5%. The total uncertainty in inlet temperature, considering sensor accuracy, control stability, and spatial variation, was estimated to be ±0.15 °C. The purity of n-heptane and ammonia used in the experiment was 99.99% and 99.999%, respectively. Specific experimental conditions can be found in the SM. The ammonia blending ratio was defined using the following equation:

$$X_{NH_3} = \frac{V_{NH_3}}{V_{NH_3} + V_{nC_7H_{16}}} \quad (1)$$

where V_{NH3} and V_{nC7H16} represent the gas volume fractions of ammonia and n-heptane, respectively.

While temperature distribution was collected using K-type thermocouples, and the camera was used to capture images of the flames. Since planar flame fronts are highly sensitive to flow fields and thermal boundaries, maintaining a consistent temperature in the asymptotically adapted channel is crucial for achieving a stretch-free planar flame. Under specific conditions, the LBV was determined using a stable planar flame in the expanding channel. A Python script was employed to uniformly process all the captured images and accurately identify the edge position of the planar flame. The LBV of a given mixture at different initial temperatures was calculated using the following equation:

$$S_u = U_{inlet} \frac{A_{mlet}}{A_f} \frac{T_u}{T_u^0} \quad (2)$$

where U_{inlet} is the velocity of the gas mixture at the inlet section (x = 0), A_{inlet} is the cross-sectional area of the inlet section of the diverging channel, A_f is the cross-sectional area at the flame position, T_u is the initial temperature of the unburned gas mixture, and T_u^0 is the reference initial gas temperature (298 K). The overall uncertainty in LBV for this study is calculated based on previous work, which showed that the LBV difference between a flame with a strain rate of 50 s^{-1} and a non-stretching flame can be kept under 4%. As a result, the total error is controlled within ±6% [29, 52].

3. Results and discussion

3.1 Validation of mechanism

The EHDC method, which employs vaporized premixing of liquid fuels, enables the measurement of LBV over a wide temperature range at atmospheric pressure. Fig. 3 shows that the LBV measured using this method agree well with published data.Specifically, for Φ = 1.1, the measured value was 1.5% lower than the result obtained by Kumar et al. using the counterflow flame method [54]. Meanwhile, it was 4.4% and 10% higher than the measurements by Dirrenberger [26] and Sileghem [27] (reproduced from Konnov et al.[52]) respectively, acquired via the heat flux method. It should be noted that this method is prone to flame lift-off and flashback when measuring lean and rich mixtures, making it difficult to establish a stable laminar flame within the channel.

The updated and original mechanisms both effectively reproduce the LBV profiles of n-heptane, with the revised mechanism producing slightly elevated predictions under fuel-rich conditions compared to its predecessor. The refined mechanism further demonstrates consistency with both the counterflow flame structure and current experimental data.

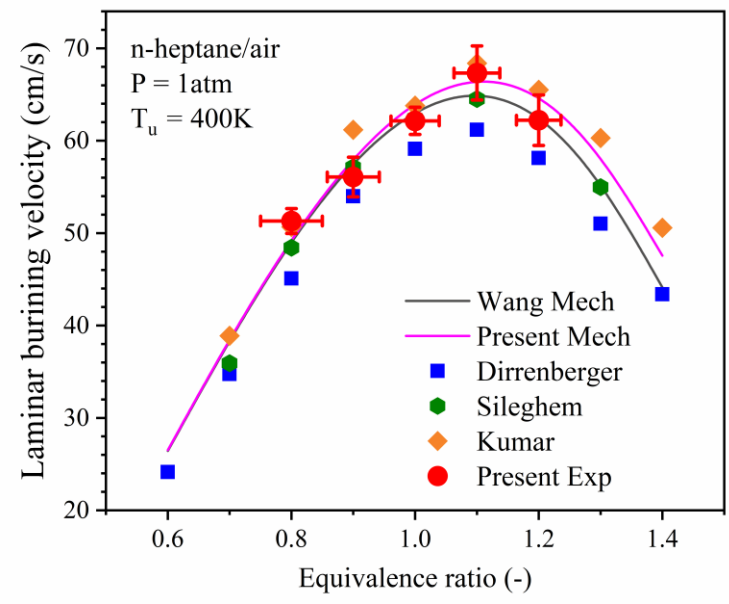

Fig. 3 Comparison chart of LBV experimental results for n-heptane [26, 27, 54]

To comparatively analyze prediction discrepancies among different skeletal mechanisms, Fig. 4 presents predicted LBV for pure n-heptane and 50% ammonia-blended fuel under identical conditions. Considering comprehensive mechanisms are computationally prohibitive for practical engine simulations, this analysis therefore focuses on existing reduced skeletal mechanisms relevant to practical implementations. When compared to the n-heptane baseline case presented in Fig. 4(a), the ammonia addition scenario (Fig. 4(b)) reveals substantial variations in predictive accuracy among the evaluated mechanisms. The Alekseev mechanism demonstrates overprediction of LBV under lean-fuel conditions, with maximum deviations reaching 9% relative to experimental data (X_{NH3} = 50%, Φ = 0.9), despite being the most compact chemical kinetic model. The Ou mechanism underpredicts LBV by approximately 4 cm/s under fuel-lean conditions (X_{NH3} = 50%, Φ from 0.8 to1.1) while maintaining reasonable agreement under rich combustion environments. The Wang and Xu mechanisms exhibit similarity in predictions due to comparable kinetic frameworks; however, both show deviations exceeding 5% from experimental measurements under fuel-rich conditions (Φ = 1.1). The current mechanism demonstrates superior performance in predicting stoichiometric and fuel-lean premixed fuel behavior. As Wang et al. [35] pointed out, the C-N interaction reaction primarily affects the predicted LBV values when Φ ≥ 1.0. Meanwhile, the current mechanism improves the prediction accuracy of LBV near stoichiometric conditions, resulting from enhanced modeling of C-N related reactions. The minor over-prediction observed in the Φ = 1.2 regime may be attributed to the current mechanism's enhanced inclusion of NH_2 sub-reactions, particularly those involving HO_2 radicals, which leads to an overestimation of ammonia's reactivity under fuel-rich

conditions. Overall, the proposed mechanism accurately capturing flame propagation characteristics at high ammonia fraction ratios, especially in the vicinity of the stoichiometric ratio (Φ from 0.8 to1.1).

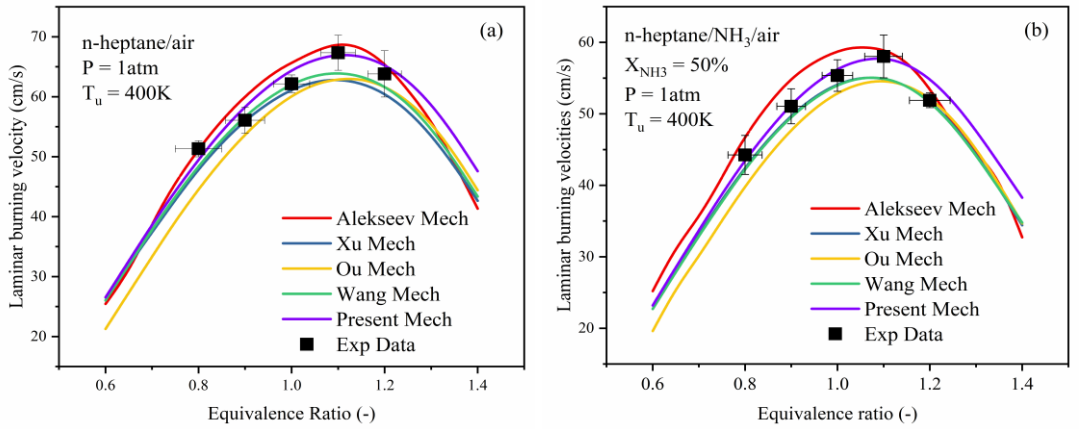

Fig. 4 Comparison chart of LBV simulation results based on different structural mechanisms (a) n-heptane ; (b) X_{NH3} = 50%

To validate the impact of refined C-N interactions on n-heptane oxidation kinetics, Fig. 5 compares ignition delay time (IDT) predicted by present skeletal mechanisms against experimental data from Fieweger et al. [55, 56], Heufer and Olivier [57]. Simulations exhibit good agreement with experiments, though the current mechanism yields lower IDT predictions at elevated temperatures (T ≥ 1250 K) among them. This discrepancy may due to the increased reaction rate of R395 relative to the base mechanism. Predictions across other temperature regimes generally align with Wang mechanism. Regarding ammonia/n-heptane blended fuels, in fig.5(b), the current mechanism captures IDT trends adequately but fails to accurately reproduce absolute IDT magnitudes from Yu et al. [11], Song et al. [58] and Ji et al. [34]. While most simulations employ volume profile methods (VPRO) for RCM data, conventional constant-volume approaches (CONV) show significant variations in IDT calculations for ammonia-blended fuels [58]. Furthermore, the framework mechanism is also considered to have certain limitations in the prediction of negative temperature coefficient (NTC) region of binary fuel mixture[19]. Collectively, modified C-N reactions exert negligible influence on low-to-medium temperature ignition of fuel blends.

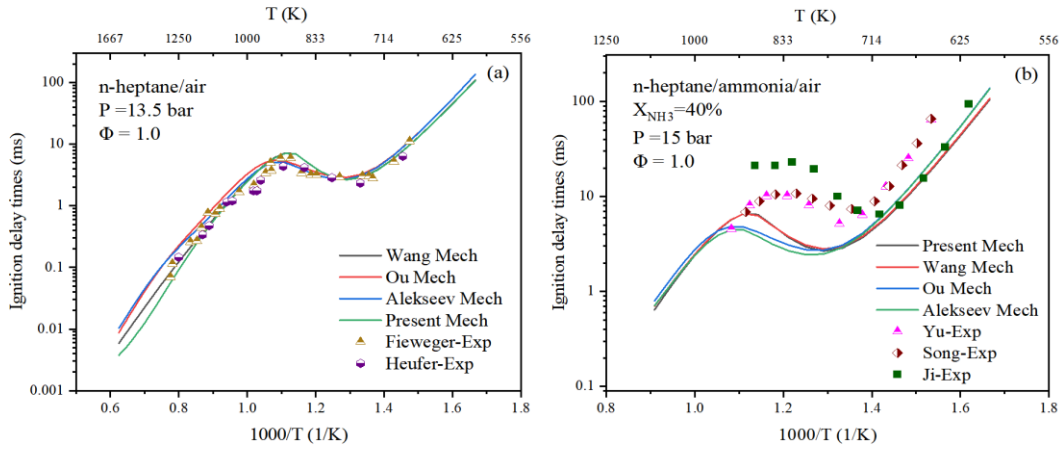

Fig. 5 Comparison of IDT experimental and simulation results (a)n-heptane;(b)X_{NH3} = 50%

3.2 LBV of n-heptane/ammonia blend fuels

Fig. 6 synthesizes LBV variations with ammonia fraction across equivalence ratios in this study, revealing a monotonic LBV decrease at preheating temperatures of 400 K and 500 K with ascending ammonia blending ratios. At 400 K preheat and Φ = 1.1, elevating X_{NH3} from 0 to 0.7 reduces laminar burning velocity from 67.33 cm/s to 52.60 cm/s, corresponding to a 22% reduction. At 500 K with Φ = 1.1, X_{NH3} = 0.7 augmentation effects a 21% LBV decline, whereas 4.4% and 14% reductions occur for 0-0.3 and 0-0.5 X_{NH3} increments respectively. To quantify X_{NH3} impacts on LBV, the reduction profile bifurcates into two distinct regimes: linear LBV diminution dominates at low-to-medium X_{NH3}, transitioning to exponential decay beyond a critical threshold. Previous studies [19] have considered the influence of ammonia mass fraction on the LBV of the mixture to be linear. While exploring this two-stage characteristic of ammonia volume fraction is of great significance for understanding the chemical transformation of the mixed fuel from the main carbon-hydrogen molecular pathway to the N-related molecule at the molecular weight level. Notably, the nonlinear suppression of LBV occurs even at mass fractions corresponding to X_{NH3} = 0.5 (≈14.4 wt%), indicating a kinetic shift beyond simple dilution effects. To facilitate a more accurate quantitative description, fitting functions exemplifying this behavior are tabulated in Table 3, with correlation coefficient exceeding 99.5%. The transition point for Φ = 1.1 is X_{NH3} = 0.5, similar trends can also be observed in Fig. 6 at other equivalent. This validates the feasibility of predicting LBV at specific Φ and X_{NH3} via fitted functions.

Table 3 S_u-X_{NH3} function fitting relationship equation

Φ	**T_u [K]**	**X_{NH3}**	**S_u (X_{NH3}) [cm/s]**	**correlation coefficient**
1.1	400	[0,0.5]	S_u = -18.14 X_{NH3} + 67.26	R^2 = 99.68
		(0.5,0.95]	S_u = -0.02132*exp(X_{NH3}) + 56.88	R^2 = 99.93
	500	[0,0.5]	S_u = -26.22 X_{NH3} + 99.04	R^2 = 99.59
		(0.5,0.95]	S_u = -0.006836*exp(X_{NH3}) +	R^2 = 99.80

Φ	T_u [K]	X_{NH3}	S_u (X_{NH3}) [cm/s]	correlation coefficient
			86.41	

Notably, whereas Φ = 1.1 yields higher LBV than other conditions experimentally, at X_{NH3} = 0.85, peak burning velocity may emerge between Φ = 1.0 and 1.1, consistent with Φ = 1.05 maxima reported for pure ammonia flames [59, 60].

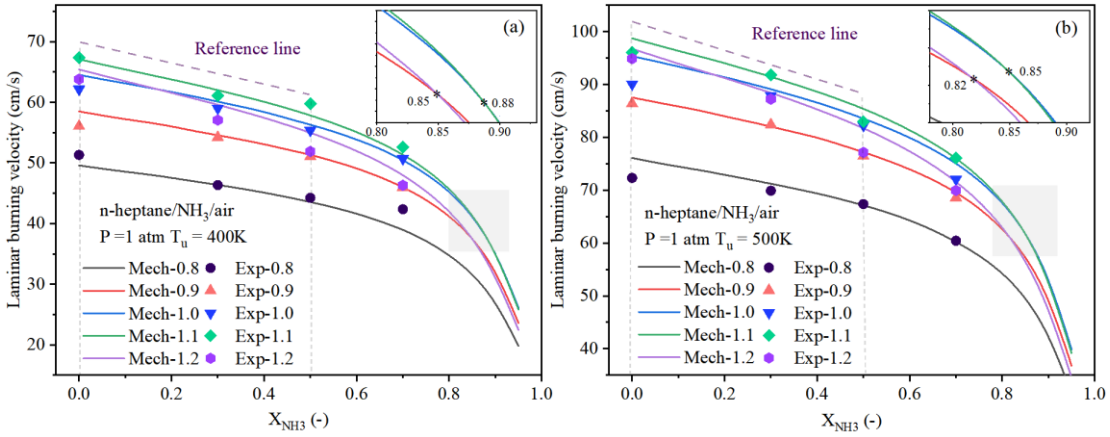

Fig. 6 The evolution trend of LBV with X_{NH3} (a) T_u = 400 K;(b) T_u = 500 K

Fig. 7 illustrates that increases in the ammonia fraction progressively decrease the adiabatic flame temperature (AFT), demonstrating a positive AFT-LBV correlation. The peak AFT occurs at Φ = 1.0 for high X_{NH3} as it primarily reflects heat release characteristics during combustion, thermal diffusion rates, and chemical kinetic parameters. However, previous studies [53] highlight that reaction pathways and mass transfer mechanisms significantly influence the final LBV, and a quantitative study was conducted. With ammonia participating in C-N reactions during combustion [61], thereby exerting additional chemical effects that reduce LBV. Conversely, under slightly rich conditions (Φ = 1.1), the elevated LBV results from increased fuel-oxidizer molecular collisions and enhanced radical interaction dynamics.

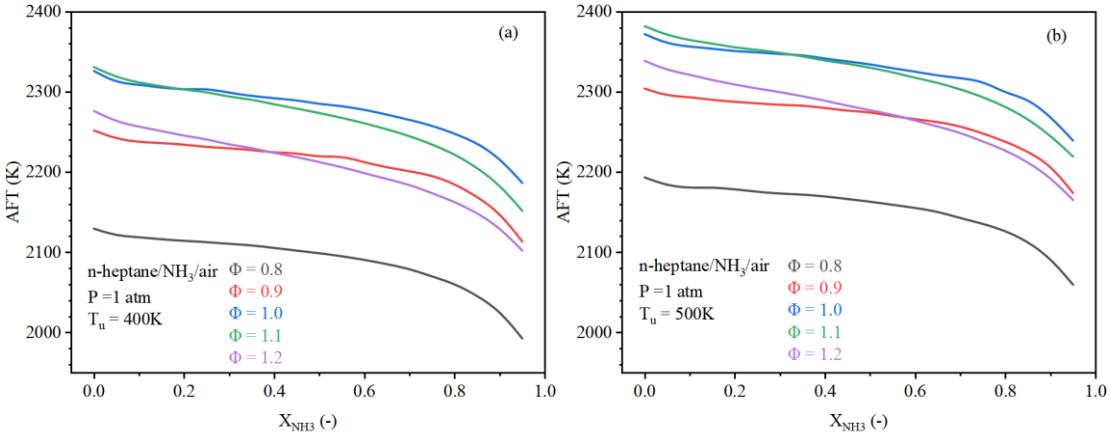

Fig. 7 The AFT results of n-heptane/ammonia at experimental conditions (a)T_u = 400 K;(b)T_u = 500 K

To assess preheating temperature effects on LBV, Fig.8 quantifies LBV increments between 400 K and 500 K, with calculations derived from experimental measurements. Subplots (a)-(d) delineate varying ammonia fractions. LBV enhancements exhibit minimal dependence on Φ and X_{NH3}, consistently approaching 50% across all tested conditions. Regardless of temperature or ammonia concentration, LBV profiles versus equivalence ratio maintain consistent morphology, peaking near Φ = 1.1. Dugger et al. [62] pioneered the power-law correlation for this temperature-dependent behavior, formalized in Equation (3).

$$S_u = S_u^0(T_u/T_u^0)^\alpha \quad (3)$$

where S_u and T_u denote experimentally measured LBV and preheating temperature, while S_u^0 represents LBV at reference temperature T_u^0 (typically 298 K). Given $S_u \neq 0$, the temperature exponent α is determined as 1.8 herein. Equation (3) enables approximate LBV predictions across 400-500 K, yet Fig. 8 reveals such increments demonstrate non-uniform characteristics, e.g., 40% increment corresponds to α≈1.5 inducing significant predictive deviations. This yields quantitatively inferior precision compared to fitted correlations in Table 3, but still has the potential for estimation in engineering applications.

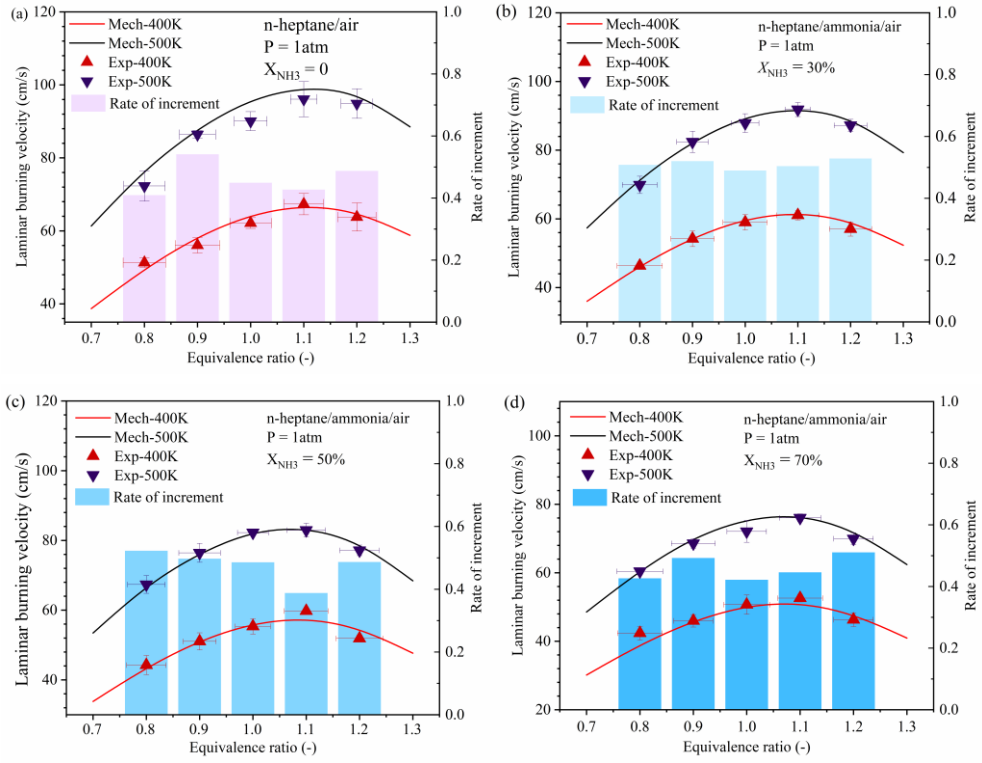

Fig. 8 The increment of LBV with T_u from 400-500 K at Φ (0.8-1.2)
(a) X_{NH3} = 0%; (b) X_{NH3} = 30%; (c) X_{NH3} = 50%; (d) X_{NH3} = 70%

3.3 Sensitivity analysis

To identify the dominant reaction pathways and key intermediate species that control flame propagation characteristics under the investigated conditions, sensitivity analysis was performed. The definition is as follows [37],

$$S = \frac{ln(S_{L+}/S_{L-})}{ln(k_+/k_-)} \quad (4)$$

where k_+ and k_- are the rates constants computeed by doubling and halving the pre-exponetial factor A according to the Arrhenius equation, with temperature exponent and activation energy held constant. S_{L+} and S_{L-} correspond to LBV at doubled and halved rates respectively. Positive sensitivity coefficient S indicates elementary reaction promotion of LBV, while negative signifies inhibition. Fig. 9 compares sensitivity responses under experimental conditions; Fig. 9 (a) indicates that for n-heptane, the R10 and R21 within H/O sub-mechanisms demonstrates high sensitivity to LBV due to OH radical generation promoting dehydrogenation and chain scission. This observation suggests a strong correlation between LBV and the H/O free radical pool [63]. Conversely, CH_3/H combination reactions like R124 and R90 reduce radical pools, thus inhibiting LBV. Subplot (b) demonstrates conserved sensitivity patterns pre-/post-ammonia blending, though R118 $C_2H_3 + O_2 = CH_2CHO + O$ sensitivity increases. This arises from diminished hydrogen abstraction in blended fuel, where oxidation becomes rate-limiting. Both this reaction and R32 HCO + M = H + CO + M show higher sensitivity coefficients under fuel-rich/lean than stoichiometric conditions. R10 sensitivity escalates sharply with decreasing oxygen content. Subplot (c) indicates temperature elevation near-proportionally amplifies key reaction sensitivities. Meanwhile higher ammonia fractions intensify H/O elementary reaction sensitivities while diminishing C-involving reaction impacts as shown in Fig. 9(d). Remarkably, R34 HCO + H = CO + H_2 inhibition strengthens at low X_{NH3}, as active NH_3 dissociation at low blending maintains crucial H-radical pools which is considered to play a dominant role in the propagation of ammonia flames [64]. Enriched X_{NH3} reduces carbon intermediates like C_2H_3 and CH_3, whereupon R124 and R90 sensitivity attenuates. The C-N reactions do not rank among the top sensitivity determining pathways, indicating that its effect on LBV is not achieved through a single reaction, but rather through the regulation of key intermediate radical pools.

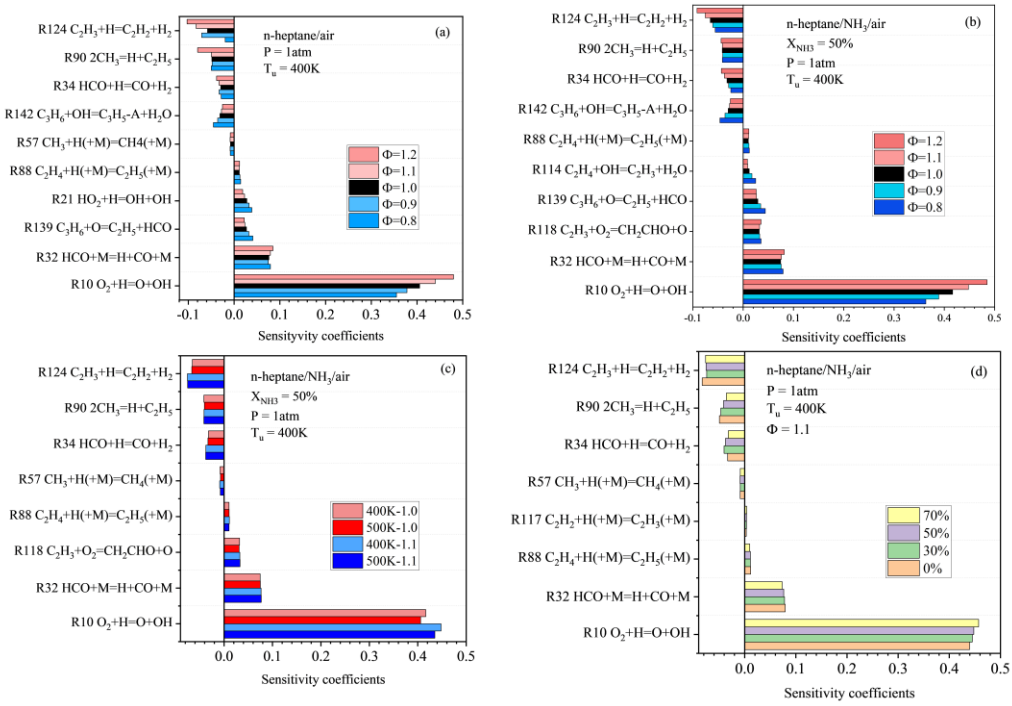

Fig. 9 The sensitivity analysis under different conditions
(a) n-heptane with Φ (0.8-1.2); (b) X_{NH3} = 50% with Φ (0.8-1.2); (c) X_{NH3} = 50% with Φ (1.0-1.1) and T_u (400K-500K); (d) Φ = 1.1 with X_{NH3} = 0-70%

3.4 Rate of production analysis

To elucidate the indirect influence of the C–N reaction, ROP analysis remains essential to trace formation routes of pivotal intermediates. Fig. 10 illustrates that radical species (OH/H/O/H_2) dynamically participate throughout fuel/intermediate oxidation processes [34], NH_3 oxidation persists marginally longer than n-heptane decomposition. During terminal oxidation stages, OH/H/O radicals attain concentration maxima followed by progressive depletion [65]. Comparatively, C-N radicals exhibit shorter activity time windows. NH_2/CH_3/C_2H_5 constitute primary fuel-derived radicals. HCN demonstrates prolonged presence with higher peak concentration among key C-N intermediates. Within the current mechanism, the C-N sub reaction R341-R498 set governs critical interactions, collectively determine the cross-interaction behavior between carbon and nitrogen species during combustion.

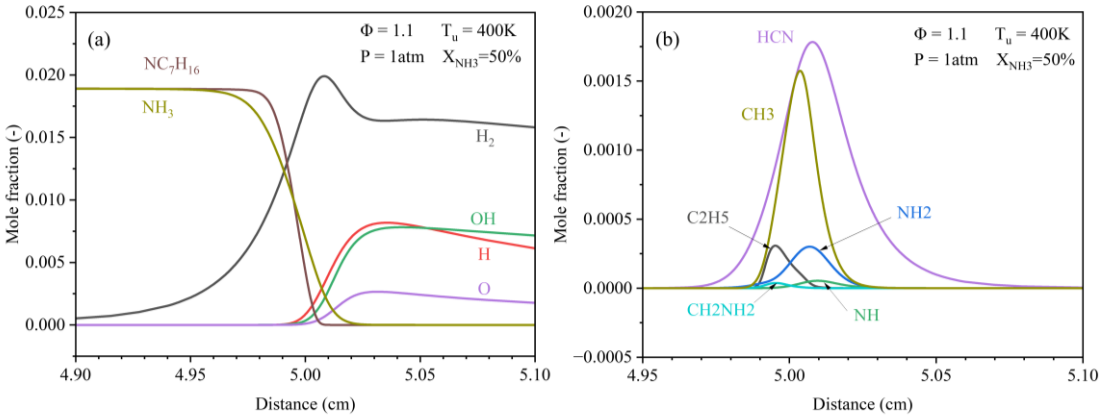

Fig. 10 Changes in the mole fraction of the main species (a) Fuel and H/O radicals; (b) C or N based radicals

Fig. 11 presents ROP analysis for key nitrogenous species: NH_2, NH, CH_2NH_2, and HCN. NH_2 predominantly forms through OH/H radical attacks on NH_3, but depletes via HCO/NH formation pathways. Comparatively, NH radicals, markers of ammonia combustion [66], exhibit simplified formation/consumption routes, primarily involving hydrogen abstraction and H-stripping reactions, following unidirectional $NH_2 \rightarrow NH \rightarrow N$ conversion. CH_2NH_2 emerges chiefly from H-exchange between C_2H_5 and NH_2, though sequential H/O_2 radical attacks consume it phase-dependently. Consequently, it maintains low steady-state concentrations as seen in Fig.10. Regarding HCN, Fig. 11d illustrates significant variations in its net production rate. he profile exhibits a distinct biphasic behavior: an initial positive peak indicating rapid generation via the dehydrogenation of intermediates (such as H_2CN and HCNN), followed by a negative region where consumption dominates. In this consumption zone, HCN is primarily attacked by O/OH radicals, decomposing into NH and CO to facilitate downstream small-molecule oxidation.

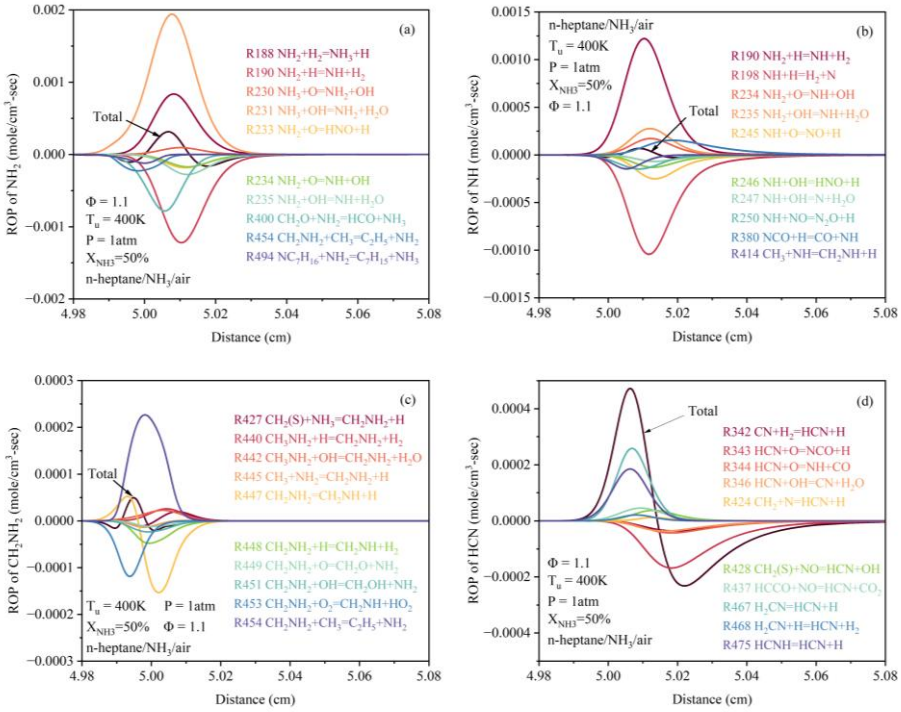

Fig. 11. ROP of main radicals in n-dodecane/ammonia flames. (a) NH_2; (b) NH; (c) CH_2NH_2; (d) HCN

Synthesizing preceding analyses, HCN functions as a pivotal C-N intermediate participating in CO/NH precursor formation, thereby enabling co-reaction of C-N groups. Its formation pathway evolution critically informs ammonia-blended combustion characteristics. Fig. 12(a) delineates NH_2 to HCN conversion routes across equivalence ratios, revealing that: $NH_2 \rightarrow CH_3NH_2$ (CH_2NH_2) $\rightarrow CH_2NH \rightarrow HCNH \rightarrow HCN$ route dominates, whereas, N-radical pathway flux $NH_2 \rightarrow NH \rightarrow N \rightarrow H_2CN \rightarrow HCN$ intensifies with rising Φ. Enhanced reactivity at higher Φ, accelerates OH radical generation, quickening H consumption and boosting $NH \rightarrow N$ flux. NH radicals signify key ammonia reaction zone markers [66, 67]. Specifically, fuel-rich conditions promote R416 $CH_3 + N = H_2CN + H$ and R467 $H_2CN = HCN + H$. Alternative pathways include, $NH \rightarrow CH_2CN$ transitioning, though exhibiting substantial reverse flux. Crucially, as Φ increases from 0.9-1.1, C-N pathway flux drops 8.7%, while N-radical route surges 15.8%. This can explain that the differences in LBV among different Φ in Fig. 6 gradually decrease as X_{NH3} increases, because the ammonia reaction pathway becomes more prominent. Declining C-N interactions correspond to accelerated R10 $O_2 + H = O + OH$ under slightly rich conditions, reducing hydrocarbon radical dependence in ammonia oxidation.

Fig. 12(b) tracks $C_2H_5 \rightarrow HCN$ conversion against X_{NH3}. Unlike NH_2 multi-route conversion, consistent with reports that enhanced ammonia input negligibly alters N-incorporation routes [68]. C_2H_5/CH_3 exclusively proceed via $CH_2NH_2 \rightarrow CH_2NH \rightarrow HCNH \rightarrow HCN$ amid intense competition with HCO pathways. As noted in ROP analysis, HCO formation consumes NH_2, thereby diminishing $NH_2 \rightarrow HCN$ flux. Elevated X_{NH3} increases, NH_2 concentrations, intensifying reverse R454 $CH_2NH_2 + CH_3 = C_2H_5 + NH_2$. This elevates $C_2H_5 \rightarrow CH_2NH_2$ flux. Concurrently,

CH_3 radical pools deplete at higher X_{NH3}, lowering R445 $CH_3 + NH_2 = CH_2NH_2 + H$ preference. Consequently, $CH_3 \rightarrow CH_2NH_2$ conversion flux decreases.

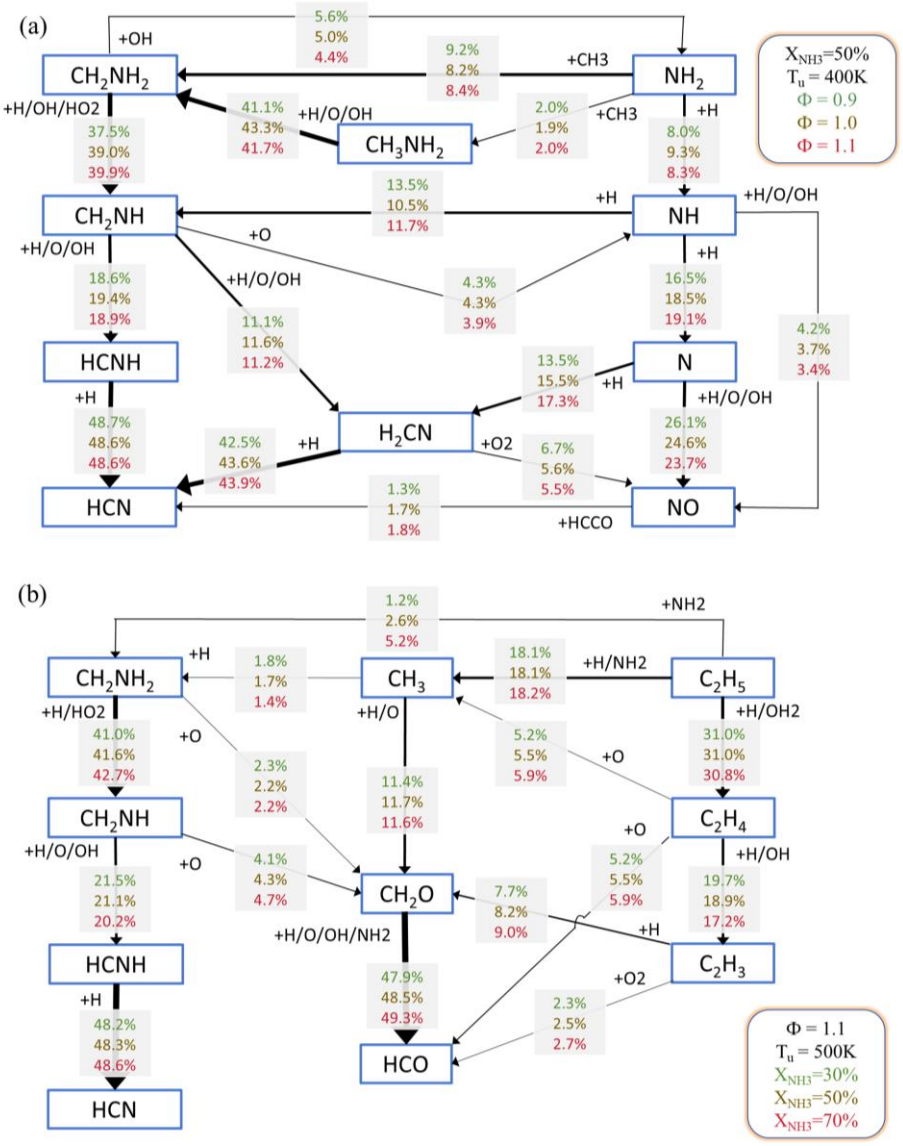

Fig. 12 Reaction path analysis. (a) $NH_2 \rightarrow$ HCN, differ in Φ (0.9-1.1); (b) $C_2H_5 \rightarrow$ HCN, differ in X_{NH3} (30%-70%)

4. Conclusions

In this study, the LBV of n-heptane/ammonia/air mixtures were systematically investigated using the EHDC method combined with numerical simulations. A skeletal kinetic model incorporating updated NH_2 sub-mechanism and C-N coupling chemistry was developed and validated against the measured LBV data. The LBV were measured across a wide range of X_{NH3}, T_u and Φ. The evolution of key C-N intermediate species and the transition of dominant reaction pathways were further elucidated. The main conclusions drawn are as follows:

1. Improved mechanism result in a 5% enhancement in agreement with present experiment,

indicating that the updated kinetic model demonstrates enhanced predictive capability for LBV under high-ammonia blending ratios and thermally elevated conditions.

2. The nonlinear attenuation trend of LBV with respect to the X_{NH3} was analyzed, exhibiting a biphasic decay pattern with increasing X_{NH3}, that an initial linear reduction (X_{NH3} < 50%) transitions to exponential decay at higher X_{NH3}. The mixture LBV reaches peak at Φ = 1.1 under investigated conditions. Increasing premix temperature from 400 K to 500 K enhances LBV by approximately 50% across various X_{NH3} and Φ.

3. LBV exhibits a positive correlation with the concentrations of active radical pools H, O, and OH; following ammonia blending, the inhibitory effect of H-abstraction reactions on LBV attenuate while the sensitivity of oxygen-related reactions intensifies. T_u and Φ monotonically modulate the sensitivity of critical reactions. HCN, NH_2, CH_3, and C_2H_5 constitute the primary fuel-derived intermediate radical species, among which HCN generation involves diverse pathways, yet HCO demonstrates competitive interaction with its formation mechanisms; as Φ and X_{NH3} increase, the $NH_2 \rightarrow$ HCN conversion pathway transitions from the C-N pathway to the N pathway.

These findings provide a fundamental basis for developing predictive models of ammonia-hydrocarbon combustion, with direct implications for optimizing flame propagation characteristics in ammonia-diesel dual-fuel systems across extended operational ranges.

Declaration of competing interest

The authors declare that they have no known competing financial interests or personal relationships that could have appeared to influence the work reported in this paper.

Acknowledgements

This work was supported by International Science and Technology Cooperation Program of Jiangxi Province (20253BDH410011), the Science and Technology Planning Project of Guangdong Province, China (No. 2024A0505040019), Guangdong Basic and Applied Basic Research Foundation (No. 2023B1515120012) and Science and technology innovation project for carbon peak and carbon neutrality of Jiangxi Carbon Neutralization Research Center (2022JXST03) .

References

[1] Valera-Medina A, Xiao H, Owen-Jones M, David WIF, Bowen PJ. Ammonia for power. Progress in Energy and Combustion Science 2018;69:63-102.

[2] Bora BJ, Sharma P. Towards sustainable and explainable dual-fuel diesel engine modeling:a SHAP-Based evaluation of Ammonia, Biogas, and hydrogen combustion dynamics. Energy Conversion and Management 2026;351:121014.

[3] Zhang X, Moosakutty SP, Rajan RP, Younes M, Sarathy SM. Combustion chemistry of ammonia/hydrogen mixtures: Jet-stirred reactor measurements and comprehensive kinetic modeling. Combustion and Flame 2021;234:111653.

[4] Huang Y, Xu C, Li Y, Li H, Gu Z, Deng H, et al. Enhancing ammonia combustion: Study of laminar burning velocity, flame instability, and NOx emissions under oxygen-enriched conditions. Journal of the Energy Institute 2026;125:102424.

[5] Xu L, Miccio M, Dong P, Zhang Z, Long W, Bai X-S. Combustion and emission characteristics in a two-stroke direct-injection compression-ignition ammonia/diesel dual-fuel engine. Fuel 2026;422:139142.
[6] Wang Q, Wang Y, Zhou Y, Hao Y, Long W, Tian H, et al. Impact of diesel post-injection strategy on combustion and emission characteristics of a high-speed ammonia/diesel dual direct-injection engine. Energy 2025;338:138777.
[7] Meng Q, Wang H, Huang Z, Luo K, Fan J. Direct numerical simulation of ammonia spray combustion ignited by n-heptane flame under high-pressure conditions. Applications in Energy and Combustion Science 2025;23:100343.
[8] Hu Z, An Y, Pei Y, Zhao D, Zhao H, Shi H. Development of a chemical kinetic mechanism for ammonia/macromolecular hydrocarbon combustion. Fuel 2024;368:131618.
[9] Liu Z, He X, Feng G, Zhao C, Zhou X, Wang Z, et al. Experimental and kinetic study on the laminar burning velocity of TRF/NH3-air premixed flame at elevated pressure. Fuel 2024;366:131256.
[10] Fakhari AH, Gharehghani A, Salahi MM, Andwari A. A chemical kinetic mechanism for ammonia/natural gas/diesel blends: Development, optimization and multi-scale validation. Chemical Engineering Journal 2026;530:172433.
[11] Yu L, Zhou W, Feng Y, Wang W, Zhu J, Qian Y, et al. The effect of ammonia addition on the low-temperature autoignition of n-heptane: An experimental and modeling study. Combustion and Flame 2020;217:4-11.
[12] Zhang K, Banyon C, Bugler J, Curran HJ, Rodriguez A, Herbinet O, et al. An updated experimental and kinetic modeling study of n-heptane oxidation. Combustion and Flame 2016;172:116-35.
[13] Glarborg P, Miller JA, Ruscic B, Klippenstein SJ. Modeling nitrogen chemistry in combustion. Progress in Energy and Combustion Science 2018;67:31-68.
[14] Pan J, Tang R, Wang Z, Gao J, Xu Q, Shu G, et al. An experimental and modeling study on the oxidation of ammonia and n-heptane with JSR. Proceedings of the Combustion Institute 2023;39(1):477-85.
[15] Thorsen LS, Jensen MST, Pullich MS, Christensen JM, Hashemi H, Glarborg P, et al. High pressure oxidation of NH3/n-heptane mixtures. Combustion and Flame 2023;254:112785.
[16] Dong S, Wang B, Jiang Z, Li Y, Gao W, Wang Z, et al. An experimental and kinetic modeling study of ammonia/n-heptane blends. Combustion and Flame 2022;246:112428.
[17] Fang Y, Qu W, Feng L. Experimental and kinetic modeling study on auto-ignition of ammonia/n-heptane mixtures at intermediate temperatures. Combustion and Flame 2024;265:113488.
[18] Xu L, Chang Y, Treacy M, Zhou Y, Jia M, Bai X-S. A skeletal chemical kinetic mechanism for ammonia/n-heptane combustion. Fuel 2023;331:125830.
[19] Alekseev VA, Nilsson EJK. Reduced kinetics of NH3/n-heptane: Model analysis and a new small mechanism for engine applications. Fuel 2024;367:131464.
[20] Ou J, Yang R, Yan Y, Liu J, Liu Z, Liu J. Chemical mechanism development for ammonia/n-heptane blends in dual fuel engines. Journal of the Energy Institute 2025;120:102077.
[21] Mao G, Liu X, Mei D, Li R, Zhang P. Data-validated surrogate modeling of ignition delay for ammonia/n-heptane gas mixtures using a physics-consistent data-driven approach. Journal of Industrial and Engineering Chemistry 2026.
[22] Han X, Wan K, Nagy T. A novel data consistency analysis for experimental laminar burning velocities of NH3-H2 mixtures. Combustion and Flame 2026;286:114855.
[23] Han X, Xu L, Qian Y. Laminar burning velocities of toluene, TRF, and PRF flames: More reliable datasets for model validations including ultra-lean conditions. Combustion and Flame 2026;284:114691.
[24] Cakir BO, Sanned D, Prakash M, Brackmann C, Richter M, Fureby C. Application and assessment of background oriented Schlieren for laminar burning velocity measurements. Experimental Thermal and Fluid Science 2025;163:111357.
[25] Kumar K, Sung C-J. Laminar flame speeds and extinction limits of preheated n-decane/O2/N2 and n-dodecane/O2/N2 mixtures. Combustion and Flame 2007;151(1):209-24.
[26] Dirrenberger P, Glaude PA, Bounaceur R, Le Gall H, da Cruz AP, Konnov AA, et al. Laminar burning velocity of gasolines with addition of ethanol. Fuel 2014;115:162-9.
[27] Sileghem L, Alekseev VA, Vancoillie J, Van Geem KM, Nilsson EJK, Verhelst S, et al. Laminar burning velocity of gasoline and the gasoline surrogate components iso-octane, n-heptane and toluene. Fuel 2013;112:355-65.

[28] Guo L, Zhu Y, Li D, Sun W, Shi Y, Liu C, et al. Study on the combustion characteristics and reaction mechanism of high-reactive-fuels-blended ammonia. Journal of the Energy Institute 2025;123:102270.
[29] Xie S, Li X, Li T, Huo J, Wang J, Wang C, et al. Experimental and numerical study on the laminar burning velocities of n-decane/toluene/air mixtures at elevated temperatures. Fuel 2022;322:124176.
[30] Lubrano Lavadera M, Han X, Konnov AA. Comparative Effect of Ammonia Addition on the Laminar Burning Velocities of Methane, n-Heptane, and Iso-octane. Energy & Fuels 2020;35(9):7156-68.
[31] Liu B, Zhou M, Zhang Z, Song Q, Belal BY, Li G. Laminar Burning Velocities of Ammonia/n-Heptane/Air Mixtures at Pressures up to 1.0 MPa. Energy & Fuels 2024;38(17):16896-910.
[32] Feng Y, Zhu J, Mao Y, Raza M, Qian Y, Yu L, et al. Low-temperature auto-ignition characteristics of NH3/diesel binary fuel: Ignition delay time measurement and kinetic analysis. Fuel 2020;281:118761.
[33] Wang B, Dong S, Jiang Z, Gao W, Wang Z, Li J, et al. Development of a reduced chemical mechanism for ammonia/n-heptane blends. Fuel 2023;338:127358.
[34] Ji Z, Bao Z, Chen H, Li X, Geng L, Chen Z, et al. Kinetic modeling study of autoignition, laminar burning velocity, and emission characteristics of n-heptane/ammonia mixtures. Journal of Advanced Research 2025.
[35] Wang H, Chang Y, Sun K, Jia M, Wang T. Development of a reduced chemical kinetic mechanism for ammonia/diesel combustion over a wide range of ammonia energy ratios. Fuel 2025;381:133536.
[36] Nonomura K, Hori T, Yang Y, Sawada S, Akamatsu F. The effect of hydrocarbon–NOx interactions in the low-to-intermediate temperature range on the prediction of combustion behavior in a 10 kW ammonia/City gas co-firing furnace. Fuel 2026;416:138441.
[37] Ge Y, Ma H-H, Jiao Y, Yang S, Chen J-H, Wang L-Q. Combustion reaction mechanism of C0-C3/N2O flames: Experimental and kinetic modeling study of laminar burning velocity. Combustion and Flame 2026;288:114948.
[38] Chang K, Gu M, Wang Y, Zou S, Ouyang Z, Han Y, et al. Investigation of soot and NO formation pathway and the interaction between C–N species in ammonia-doped ethylene co-flow diffusion flames. Combustion and Flame 2026;285:114727.
[39] Yan T, Li K, Zhong S, Zhou D, Lu X. Study on interactions of nitrogen–hydrocarbon reaction pathways in soot formation of ammonia-doped flames. Fuel 2026;403:135971.
[40] Hamdi F, Molima S, Hamdi T, Chrigui M. Eulerian–Lagrangian study of the effects of piston geometry on liquid spray and combustion of ammonia–diesel dual-fuel engine. Applied Thermal Engineering 2026;285:129284.
[41] Zhao W, Yan F, Chen L. Numerical study of multi-stage diesel injection on the combustion characteristics of ammonia-fueled RCCI engine. Fuel 2026;412:138175.
[42] Mao G, Fu R, Mei D, Li R, Zhang P. Kinetic modeling and optimization of ammonia/n-heptane combustion for HCCI engine applications. International Journal of Hydrogen Energy 2025;187:152107.
[43] Chang Y, Jia M, Wang P, Niu B, Liu J. Construction and derivation of a series of skeletal chemical mechanisms for n-alkanes with uniform and decoupling structure based on reaction rate rules. Combustion and Flame 2022;236:111785.
[44] Stagni A, Cavallotti C, Arunthanayothin S, Song Y, Herbinet O, Battin-Leclerc F, et al. An experimental, theoretical and kinetic-modeling study of the gas-phase oxidation of ammonia. Reaction Chemistry & Engineering 2020;5(4):696-711.
[45] Zhan H, Li S, Yin G, Hu E, Huang Z. Experimental and kinetic study of ammonia oxidation and NOx emissions at elevated pressures. Combustion and Flame 2024;263:113129.
[46] Zhang Y, Zhou W, Yu L, Li Y, Lu X. Exploring the Interaction Chemistry of Ammonia with n-Hexadecane over Wide Pressure Ranges: An Experimental and Kinetic Modeling Study. Energy & Fuels 2024;38(18):17948-64.
[47] Zhan H, Shen S, Yin G, Bao Y, Hu E, Huang Z. High-Pressure Oxidation of an Ammonia–Methanol Mixture: An Experimental and Modeling Study. Energy & Fuels 2024;38(23):23091-100.
[48] Klippenstein SJ, Glarborg P. Theoretical kinetics predictions for NH2 + HO2. Combustion and Flame 2022;236:111787.
[49] Akram M, Kumar S. Experimental studies on dynamics of methane–air premixed flame in meso-scale diverging channels. Combustion and Flame 2011;158(5):915-24.

[50] Akram M, Kumar S. Measurement of Laminar Burning Velocity of Liquified Petrolium Gas Air Mixtures at Elevated Temperatures. Energy & Fuels 2012;26(6):3267-74.
[51] Akram M, Minaev S, Kumar S. Investigations on the Formation of Planar Flames in Mesoscale Divergent Channels and Prediction of Burning Velocity at High Temperatures. Combustion Science and Technology 2013;185(4):645-60.
[52] Konnov AA, Mohammad A, Kishore VR, Kim NI, Prathap C, Kumar S. A comprehensive review of measurements and data analysis of laminar burning velocities for various fuel+air mixtures. Progress in Energy and Combustion Science 2018;68:197-267.
[53] Chen D, Zhang J, Li J, Li X, Huang H, Kobayashi N, et al. Experimental and numerical study on the laminar burning velocities of n-dodecane/ammonia/air mixtures. Energy 2025;326:136303.
[54] Kumar K, Freeh JE, Sung CJ, Huang Y. Laminar Flame Speeds of Preheated iso-Octane/O2/N2 and n-Heptane/O2/N2 Mixtures. Journal of Propulsion and Power 2007;23(2):428-36.
[55] Fieweger K, Blumenthal R, Adomeit G. Self-ignition of S.I. engine model fuels: A shock tube investigation at high pressure. Combustion and Flame 1997;109(4):599-619.
[56] Ciezki HK, Adomeit G. Shock-tube investigation of self-ignition of n-heptane-air mixtures under engine relevant conditions. Combustion and Flame 1993;93(4):421-33.
[57] Heufer KA, Olivier H. Determination of ignition delay times of different hydrocarbons in a new high pressure shock tube. Shock Waves 2010;20(4):307-16.
[58] Song M, Wang Q, Wang Z, Fang Y, Qu W, Gong Z, et al. Auto-ignition characteristics and chemical reaction mechanism of ammonia/n-heptane mixtures with low n-heptane content. Fuel 2024;364:131011.
[59] Goodman J, Dhankhar A, Date A, Lappas P. Ammonia–air laminar flame speeds from ambient to IC engine conditions: A review. Fuel 2025;383:133769.
[60] Zhang X, Tian J, Cui Z, Xiong S, Yin S, Wang Q, et al. Visualization study on the effects of pre-chamber jet ignition and methane addition on the combustion characteristics of ammonia/air mixtures. Fuel 2023;338:127204.
[61] Ren F, Cheng X, Gao Z, Huang Z, Zhu L. Effects of NH3 addition on polycyclic aromatic hydrocarbon and soot formation in C2H4 co-flow diffusion flames. Combustion and Flame 2022;241:111958.
[62] Dugger GL, Graab DD. Flame velocities of hydrocarbon-oxygen-nitrogen mixtures. Symposium (International) on Combustion 1953;4(1):302-10.
[63] Jiang J, Yang W, Weng W, Dai Y, Liu S, Wang S, et al. Measurement of laminar burning velocity and OH/NO concentrations in preheated partially cracked ammonia and kinetic analysis. International Journal of Hydrogen Energy 2026;234:155113.
[64] Xu C, Deng H, Huang Y, Li H, Gu Z, Kambo P, et al. Experimental and numerical simulation study on laminar burning velocity of oxygen-enriched ammonia fuel based on the constant volume method. International Journal of Hydrogen Energy 2026;216:153780.
[65] Wen M, Liu H, Cui Y, Ming Z, Wang W, Wang X, et al. A study on optical diagnostics and numerical simulation of dual fuel combustion using ammonia and n-heptane. Energy 2024;313:133977.
[66] Wang R, Zhang M, An Z, Cai X, Liu J, Wang J, et al. Topology characteristics of liquid ammonia swirl spray flame. Proceedings of the Combustion Institute 2024;40(1):105740.
[67] Aldén M. Spatially and temporally resolved laser/optical diagnostics of combustion processes: From fundamentals to practical applications. Proceedings of the Combustion Institute 2023;39(1):1185-228.
[68] Du H, Hu Y, Zhang J, Wei H, Zhou G, Bai J, et al. Effects of ammonia addition on flame temperature profiles of n-heptane laminar diffusion flames under elevated pressures. Fuel 2025;387:134391.